

Quantum charge pumping through resonant crossed Andreev reflection in superconducting hybrid junction of Silicene

Ganesh C. Paul^{1,2} and Arijit Saha^{1,2}

¹ *Institute of Physics, Sachivalaya Marg, Bhubaneswar, Orissa, 751005, India*

² *Homi Bhabha National Institute, Training School Complex, Anushakti Nagar, Mumbai 400085, India*
(Dated: October 3, 2016)

We theoretically investigate the phenomena of adiabatic quantum charge pumping through a normal-insulator-superconductor-insulator-normal (NISIN) setup of silicene within the scattering matrix formalism. Assuming thin barrier limit, we consider the strength of the two barriers (χ_1 and χ_2) as the pumping parameters in the adiabatic regime. Within this geometry, we obtain crossed Andreev reflection (CAR) with probability unity in the χ_1 - χ_2 plane without concomitant transmission or elastic cotunneling (CT). Tunability of the band gap at the Dirac point by applying an external electric field perpendicular to the silicene sheet and variation of the chemical potential at the normal silicene region, open up the possibility of achieving perfect CAR process or transmission through our setup. This resonant behavior is periodic with the barrier strengths. We analyze the behavior of the pumped charge through the NISIN structure as a function of the pumping strength and angles of the incident electron. We show that quantized pumped charge can be obtained through our geometry when the pumping contour encloses the CAR or transmission resonance in the pumping parameter space. We discuss possible experimental feasibility of our theoretical predictions.

PACS numbers: 72.80.Vp, 74.45.+c, 71.70.Ej, 73.40.Gk

I. INTRODUCTION

In recent years, a close cousin to graphene^{1,2}, silicene^{3–11} consisting of a monolayer honeycomb structure of silicon atoms, has attracted a lot of research interest in condensed matter community due to its unique Dirac like band structure which allows one to realize a rich variety of topological phases^{12–17} and Majorana fermion¹⁶ in it under suitable circumstances. Moreover, this band structure is shown to be tunable by an external electric field applied perpendicular to the silicene sheet^{18,19}. Dirac fermions, in turn, becomes massive at the two valleys \mathbf{K} and \mathbf{K}' in this material. These properties has made silicene to be a promising candidate for realizing spintronics^{20–24}, valleytronics^{14,25–27} devices as well as silicon based transistor²⁸ at room temperature.

Very recently, superconducting proximity effect in silicene has been investigated theoretically in Ref. 29–31. Although, up to now, no experiment has been put forward in the context of proximity effect in silicene. In Ref. 29, a unique possibility of acquiring pure crossed Andreev reflection (CAR) without any contamination from normal transmission/co-tunneling (CT) has been reported in normal-superconductor-normal (NSN) junction of silicene. Such pure CAR is possible to obtain by tuning the chemical potential and band gap at the two normal sides. However, in such NSN junction, maximum value of CAR probability comes out to be 96.2%. This motivates us to study a NISIN junction of silicene and explore whether incorporating an insulating barrier at each NS interface can give rise to resonant CAR in such setup.

On the other hand, adiabatic quantum pumping, is a transport phenomena in which low-frequency periodic modulations of at least two system parameters^{32–35} with

a phase difference lead to a zero bias finite dc current in meso and nanoscale systems. Such zero-bias current is obtained as a consequence of the time variation of the parameters of the quantum system, which explicitly breaks time-reversal symmetry^{36,37}. It is necessary to break time-reversal symmetry in order to get net pumped charge, but it is not a sufficient condition. Indeed, in order to obtain a finite net pumped charge, parity or spatial symmetry must also be broken. Finally, to reach the adiabatic limit, the required condition to satisfy is that the period T of the oscillatory driving signals has to be much larger than the dwell time $\tau_{dwell} \simeq L/v_F$ of the electrons inside the scattering region of length L , i.e., $T = 2\pi/\omega \gg \tau_{dwell}$ ³⁴. In this limit, the pumped charge in a unit cycle becomes independent of the pumping frequency. This is referred to as “adiabatic charge pumping”³⁴.

During the past decades, quantum charge and spin pumping has been studied extensively in mesoscopic setups including quantum dots and quantum wires both at the theoretical^{38–54} as well as experimental^{55–60} level with focus on both the adiabatic and nonadiabatic regime. In recent times, quantum pumping has been explored in Dirac systems like graphene^{36,51,52,61,62} and topological insulator^{63,64}. However, the possible quantization of pumped charge⁶⁵ during a cycle through noninteracting open quantum systems has been investigated so far based on the resonant transmission process^{36,37,44,66}. In more recent times, quantized behavior of pumped charge has been predicted in superconducting wires with Majorana fermions⁶⁷, fractional fermions³⁷ and topological insulators in enlarged parameter spaces⁶⁸. Although, till date, quantum pumping phenomena through resonant CAR process has not been investigated to the best of our knowledge.

Motivated by the above mentioned facts, in this arti-

cle, we study adiabatic quantum charge pumping through resonant CAR process or resonant transmission process, under suitable circumstances, in silicene NISIN junction. We model our pump setup within the scattering matrix formalism^{33,34} and consider the strength of the two barriers (in the thin barrier limit) as our pumping parameters. We show that CAR probability can be unity in the pumping parameter space. Moreover, resonant CAR is periodic in the pumping parameter space due to the relativistic nature of the Dirac fermions. Similar periodicity is present, in case of resonant tunneling process as well under suitable condition. Adiabatic quantum pumping through these processes with the modulation of two barrier strengths can lead to quantized pumped charge from one reservoir to the other. We investigate the nature of pumped charge through NISIN structure as a function of the pumping strength and angle of incidence of incoming electrons choosing different types of pumping contours (circular, elliptic, lemniscate³⁷ etc.).

The remainder of the paper is organised as follows. In Sec. II, we describe our pump setup based on the silicene NISIN junction and the formula for computing pumped charge within the scattering matrix framework. Sec. III is devoted to the numerical results obtained for the pumped charge as a function of various parameters of the systems. Finally, we summarize our numerical results and conclude in Sec. IV.

II. MODEL AND METHOD

In this section we describe our pump setup in which we consider a normal-insulator-superconductor-insulator-normal (NISIN) structure of silicene in $x - y$ plane as depicted in Fig. 1 with the superconducting region being located between $0 < x < L$, while the insulating regions are on its left, $-d < x < 0$, and on its right, $L < x < L + d$. The normal region of silicene occupies at the extreme left *i.e.*, $x < -d$ and extreme right ends, $x > L + d$. Here, superconductivity is assumed to be induced in the silicene sheet via the proximity effect, where a bulk s -wave superconductor is placed in close proximity to the sheet in the region $0 < x < L$. The two insulating regions in silicene have gate tunable barriers of strength χ_1 and χ_2 in the thin barrier limit^{30,31}. An additional gate voltage G can tune the chemical potential in the normal silicene region.

The silicene NISIN junction can be described by the Dirac Bogoliubov-de Gennes (DBdG) equation of the form^{29,30}

$$\begin{bmatrix} \hat{H}_{\tilde{\eta}} & \Delta \hat{1} \\ \Delta^\dagger \hat{1} & -\hat{H}_{\tilde{\eta}} \end{bmatrix} \Psi = E \Psi. \quad (1)$$

where E is the excitation energy, Δ is the proximity induced superconducting pairing gap. The Hamiltonian $H_{\tilde{\eta}}$ describes the low energy physics close to each \mathbf{K} and \mathbf{K}' Dirac points and reads as¹⁹

$$H_{\tilde{\eta}} = \hbar v_f (\tilde{\eta} k_x \hat{\tau}_x - k_y \hat{\tau}_y) + (e l E_z - \tilde{\eta} \sigma \lambda_{SO}) \hat{\tau}_z - \mu \hat{1}. \quad (2)$$

where v_f is the fermi velocity of the electrons, μ is the chemical potential, λ_{SO} is the spin-orbit term and E_z is the external electric field applied perpendicular to the silicene sheet. Here $\tilde{\eta} = \pm 1$ denotes the \mathbf{K} and \mathbf{K}' valley. In Eq. (2), σ is the spin index and $\hat{\tau}$ correspond to the Pauli matrices acting on the sublattices A and B where $\hat{1}$ is the 2×2 identity operator.

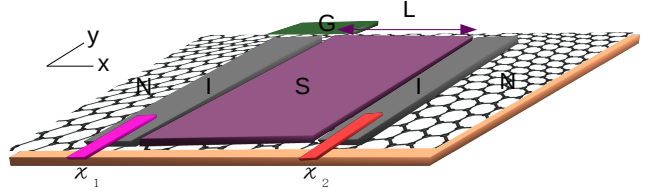


FIG. 1. (Color online) A schematic sketch of our silicene NISIN set-up. Silicene sheet with hexagonal lattice structure is deposited on a substrate (orange, light grey). Here N indicates the normal region, I denotes the thin insulating barrier region (grey, light grey). A bulk superconducting material of length L denoted by S (pink, light grey) is placed in close proximity to the silicene sheet to induce superconducting correlation in it. A gate G (dark green, dark grey) is connected to the silicene sheet to tune the chemical potential (doping) in the normal region. Two extra gates (blue and red, light grey) indicated by χ_1 and χ_2 are symbolically denoted to modulate the barrier strengths.

The potential energy term $e l E_z$ in the low energy Hamiltonian $H_{\tilde{\eta}}$ originates due to the buckled structure of silicene in which the A and B sublattices are non-coplanar (separated by a distance of length l) and therefore acquire a potential difference when an external electric field E_z is applied perpendicular to the plane. It turns out that at a critical electric field $E_z^c = \lambda_{SO}/el$, the band gap at each of the valleys become gapless with the gapless modes of one of the valley being up-spin polarized and the other being down-spin polarised^{18,19}. Away from the critical field, the bands (corresponding to $H_{\tilde{\eta}}$) at each of the valleys \mathbf{K} and \mathbf{K}' split into two conduction and valence bands with the band gap being $|e l E_z - \tilde{\eta} \sigma \lambda_{SO}|$. Note that, in silicene, the pairing occurs between $\tilde{\eta} = 1$, $\sigma = 1$ and $\tilde{\eta} = -1$, $\sigma = -1$ as well as $\tilde{\eta} = 1$, $\sigma = -1$ and $\tilde{\eta} = -1$, $\sigma = 1$ for a s -wave superconductor.

Here we set up the equations to analyze the quantum pumping phenomena through our NISIN structure. Solving Eq.(1) we find the wave functions in three different regions. The wave functions for the electrons (e) and holes (h) moving in $\pm x$ direction in left or right normal silicene region N reads

$$\psi_{Nm}^{e\pm} = \frac{1}{A} \begin{bmatrix} \pm \tilde{\eta} k_{1m}^e e^{\pm i \tilde{\eta} \alpha_{em}} \\ \tau_{1m}^e \\ 1 \\ 0 \\ 0 \end{bmatrix} \exp[i(\pm k_{1xm}^e x + k_{1y}^e y)] ,$$

$$\psi_{Nm}^{h\pm} = \frac{1}{B} \begin{bmatrix} 0 \\ 0 \\ \mp \tilde{\eta} k_{1m}^h e^{\pm i \tilde{\eta} \alpha_{hm}} \\ \tau_{1m}^h \\ 1 \end{bmatrix} \exp[i(\pm k_{1xm}^h x + k_{1y}^h y)] .$$
(3)

where the index $m = L/R$ stands for the left or right normal silicene region and we use this symbol for the rest of this section. In Eq.(3) the normalization factors are given by $A = \sqrt{\frac{2(E+\mu_m)}{\tau_{1m}^e}}$, $B = \sqrt{\frac{2(E-\mu_m)}{\tau_{1m}^h}}$ and

$$k_{1m}^{e(h)} = \sqrt{\left(k_{1xm}^{e(h)}\right)^2 + \left(k_{1y}^{e(h)}\right)^2} , \quad (4)$$

$$k_{1xm}^{e(h)} = \sqrt{(E \pm \mu_m)^2 - (elE_z - \tilde{\eta}\sigma\lambda_{SO})^2 - \left(k_{1y}^{e(h)}\right)^2} . \quad (5)$$

$$\tau_{1m}^{e(h)} = E \pm \mu_m \mp (elE_z - \tilde{\eta}\sigma\lambda_{SO}) . \quad (6)$$

Here μ_m indicates the chemical potential in the left (μ_L) or right (μ_R) normal silicene region. E is the energy of the incident particle.

Due to the translational invariance in the y -direction, corresponding momentum $k_{1y}^{e(h)}$ is conserved. Hence, the angle of incidence α_{em} and the Andreev reflection (AR) angle α_{hm} are related via the relation

$$k_{1m}^h \sin(\alpha_{hm}) = k_{1m}^e \sin(\alpha_{em}) . \quad (7)$$

In the insulating region I , the corresponding wave functions can be inferred from normal region wave functions (Eq.(3)) by replacing $\mu_m \rightarrow \mu_m - V_0(V'_0)$ where V_0 and V'_0 are the applied gate voltages at the left and right insulating regions respectively. We define dimensionless barrier strengths^{30,31} $\chi_1 = V_0 d / \hbar v_F$ and $\chi_2 = V'_0 d / \hbar v_F$ which we use as pumping parameters for our analysis. Here d is the width of the insulating barriers assumed to be the same for both of them.

In the superconducting region S , the wave functions of DBdG quasiparticles are given by,

$$\psi_S^{e\pm} = \frac{1}{\sqrt{2}} \begin{bmatrix} u_1 \\ \pm \tilde{\eta} u_1 e^{i \tilde{\eta} \theta_e} \\ u_2 \\ \pm \tilde{\eta} u_2 e^{i \tilde{\eta} \theta_e} \end{bmatrix} \exp[\pm(i\mu_S - \kappa)x + iq_y^e y] ,$$

$$\psi_S^{h\mp} = \frac{1}{\sqrt{2}} \begin{bmatrix} u_2 \\ \mp \tilde{\eta} u_2 e^{-i \tilde{\eta} \theta_h} \\ u_1 \\ \mp \tilde{\eta} u_1 e^{-i \tilde{\eta} \theta_e} \end{bmatrix} \exp[\pm(-i\mu_S - \kappa)x + iq_y^h y] \quad (8)$$

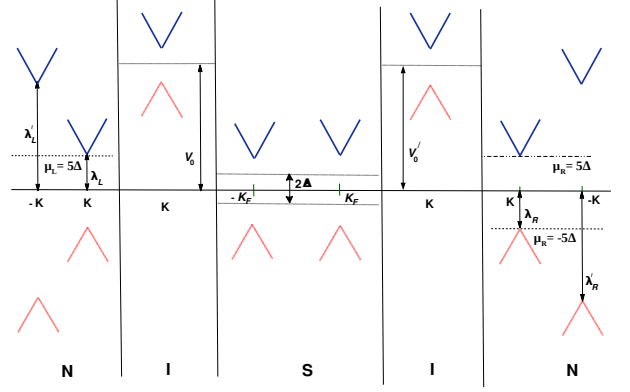


FIG. 2. (Color online) A schematic sketch of the band structure of our silicene NISIN setup is depicted. While in the normal regions of silicene (N) as well as superconducting (S) silicene region both \mathbf{K} and \mathbf{K}' valleys are presented, only \mathbf{K} valley is shown for both the insulating regions (I) for simplicity. Blue solid line indicates the conduction band while the valence bands are represented by red solid lines. For $\mu_L = 5\Delta$ and $\mu_R = -5\Delta$, we obtain pure CAR process. On the other hand, for resonant transmission to take place, chemical potential in the right normal side is set to be $\mu_R = 5\Delta$.

Here the coherence factors are given by,

$$u_{1(2)} = \left[\frac{1}{2} \pm \frac{\sqrt{E^2 - \Delta^2}}{2E} \right]^{\frac{1}{2}} \text{ and } \kappa = \sqrt{\Delta^2 - E^2} . \quad (9)$$

As before, the translational invariance along the y direction relates the transmission angles for the electron-like and hole-like quasi-particles via the following relation given by,

$$q^\beta \sin \theta_\beta = k_{1m}^e \sin \alpha_{em} . \quad (10)$$

for $\beta = e, h$. The quasiparticle momentums can be written as

$$q^{e(h)} = \mu_S \pm \sqrt{E^2 - \Delta^2} . \quad (11)$$

where $\mu_S = \mu_m + U_0$ and U_0 is the gate potential applied in the superconducting region to tune the Fermi wave-length mismatch⁶⁹ between the normal and superconducting regions. The requirement for the mean-field treatment of superconductivity is justified in our model as we have taken $\mu_S \gg \Delta$ ^{69,70} throughout our calculation.

We consider electrons with energy E incident from the left normal region of the silicene sheet. Considering normal reflection, Andreev reflection, cotunneling (normal transmission) and crossed Andreev reflection from the interface, we can write the wave functions in five different regions of the junction as

$$\begin{aligned}
\Psi_N^L &= \psi_{NL}^{e+} + r_e \psi_{NL}^{e-} + r_A \psi_{NL}^{h-}, \\
\Psi_I^L &= p_1 \psi_{IL}^{e+} + q_1 \psi_{IL}^{e-} + m_1 \psi_{IL}^{h+} + n_1 \psi_{IL}^{h-}, \\
\Psi_S &= t_1 \psi_S^{e+} + t_2 \psi_S^{e-} + t_3 \psi_S^{h+} + t_4 \psi_S^{h-}, \\
\Psi_I^R &= p_2 \psi_{IR}^{e+} + q_2 \psi_{IR}^{e-} + m_2 \psi_{IR}^{h+} + n_2 \psi_{IR}^{h-}, \\
\Psi_N^R &= t_e \psi_{NR}^{e+} + t_A \psi_{NR}^{h+}.
\end{aligned} \tag{12}$$

where r_e , r_A , t_e , t_A corresponds to the amplitudes of normal reflection, AR, transmission and CAR in the N silicene regions, respectively. The transmission amplitudes t_1 , t_2 , t_3 and t_4 denote the electron like and hole like quasiparticles in the S region. Using the boundary conditions at the four interfaces, we can write

$$\begin{aligned}
\Psi_N^L|_{x=-d} &= \Psi_I^L|_{x=-d}, & \Psi_I^L|_{x=0} &= \Psi_S|_{x=0}, \\
\Psi_S|_{x=L} &= \Psi_I^R|_{x=L}, & \Psi_I^R|_{x=L+d} &= \Psi_N^R|_{x=L+d}.
\end{aligned} \tag{13}$$

which yields a set of sixteen linearly independent equations. Solving these equations numerically, we obtain r_e , r_A , t_e , t_A which are required for the computation of pumped charge through our setup.

In order to carry out our analysis for the pumped charge in silicene NISIN structure, we choose the two dimensionless insulating barrier strengths χ_1 and χ_2 as our pumping parameters. They evolve in time either as (off-set circular contours)

$$\begin{aligned}
\chi_1 &= \chi_0 + P \cos(\omega t - \eta), \\
\chi_2 &= \chi_0 + P \cos(\omega t + \eta),
\end{aligned} \tag{14}$$

or as (“lemniscate” contours),

$$\begin{aligned}
\chi_1 &= \chi_{1_0} + P_L \left(\cos \theta \cos \omega t - \frac{1}{2} \sin \theta \sin 2\omega t \right) / (1 + \sin^2 \omega t), \\
\chi_2 &= \chi_{2_0} + P_L \left(\cos \theta \cos \omega t + \frac{1}{2} \sin \theta \sin 2\omega t \right) / (1 + \sin^2 \omega t),
\end{aligned} \tag{15}$$

respectively. In the circular contours χ_0 and in the lemniscate contours χ_{1_0} , χ_{2_0} correspond to the mean value of the amplitude respectively, around which the two pumping parameters are modulated with time. P and P_L are called the pumping strengths for the two types of contours respectively. Furthermore, 2η and θ represent the phase offset between the two pumping signals for the circular and lemniscate contours, respectively. Here ω is the frequency of oscillation of the pumping parameters.

We, in our analysis, only consider the adiabatic limit of quantum pumping where time period of the pumping parameters $T = 2\pi/\omega$ is much larger than the dwell time $\tau_{dwell} \simeq L/v_F$ of the Dirac fermions inside the proximity induced superconducting region.

To calculate the pumped charge, we employ Brower’s formula³⁴ which relies on the knowledge of the parametric

derivatives of the S -matrix elements. Following Ref. 71, S -matrix for the NISIN structure of silicene for an incident electron with energy E can be written as

$$S = \begin{bmatrix} |r_e|e^{i\gamma_e} & |r_A|e^{i\gamma_h} & |t_e|e^{i\delta_e} & |t_A|e^{i\delta_h} \\ |r_A|e^{i\gamma_h} & |r_e|e^{i\gamma_e} & |t_A|e^{i\delta_h} & |t_e|e^{i\delta_e} \\ |t_e|e^{i\delta_e} & |t_A|e^{i\delta_h} & |r_e|e^{i\gamma_e} & |r_A|e^{i\gamma_h} \\ |t_A|e^{i\delta_h} & |t_e|e^{i\delta_e} & |r_A|e^{i\gamma_h} & |r_e|e^{i\gamma_e} \end{bmatrix}, \tag{16}$$

We write here the complex S -matrix elements S_{ij} in polar form, with modulus and phase explicitly shown, since the phase is going to play a major role in the determination of the pumped charge. For a single channel S -matrix, the formula for the pumped charge becomes⁷¹

$$\begin{aligned}
Q &= \frac{e}{2\pi} \int_0^T dt [-|r_A|^2 (\dot{\gamma}_h \cos \alpha_{hL} + \dot{\gamma}_e \cos \alpha_{eL}) \\
&\quad - |t_A|^2 (\dot{\delta}_h \cos \alpha_{hR} + \dot{\gamma}_e \cos \alpha_{eL}) \\
&\quad + |t_e|^2 (\dot{\delta}_e \cos \alpha_{eR} - \dot{\gamma}_e \cos \alpha_{eL}) \\
&\quad + \dot{\gamma}_e \cos \alpha_{eL}],
\end{aligned} \tag{17}$$

Here, we have redefined the complex scattering amplitudes r_e , t_e , r_A and t_A for conservation of probability²⁹. Furthermore, γ_e , γ_h , δ_e , δ_h are the phases of r_e , r_A , t_e and t_A respectively. α_{eL} , α_{eR} corresponds to the incident and transmitted angles of electrons while α_{hL} , α_{hR} represents the reflected and transmitted angles of holes respectively. Note that, if $\alpha_{eL} = 0$, then the last term of Eq.(17) consisting of the time derivative of reflection phase is called “*topological part*”⁴⁷ while the rest is termed as “*dissipative part*”⁴⁷.

III. NUMERICAL RESULTS

In this section we present and discuss our numerical results for the pumped charge based on Eq.(17). The quantum mechanical scattering amplitudes are all functions of the incident electron energy E , length of the superconducting silicene region L , the strengths χ_1 , χ_2 of the two thin insulating barriers, chemical potential μ_m ($m = L/R$) of the left and right normal silicene region, external electric field E_z and spin orbit coupling λ_{SO} . We denote the band gaps at the left and right normal silicene side as λ_L and λ_R respectively. In addition, we have set $\hbar = 1$ throughout our analysis.

For clarity, we divide this section into two subsections. In the first one, we discuss quantum pumping via CAR process with unit probability in the χ_1 - χ_2 plane. The second one is devoted to the discussion of the same via the perfect transmission/CT process.

A. Pumping via CAR in the χ_1 - χ_2 plane

Silicene is a material where a large value of non-local CAR process can be obtained due to its unique band

structure²⁹. The band gaps and Fermi level (chemical potential) in silicene can be tuned by applying electric field only. By tuning the both, very recently, Linder *et al.* in Ref. 29 showed that one can completely block elastic cotunneling in silicene NSN junction in the subgapped regime. Consequently, pure CAR process is possible for broad range of voltages. However, maximum probability of CAR found in Ref. 29 was $\sim 96.2\%$. Previously, similar possibility of resonant CAR was also reported in p - n junction of graphene⁷² at a specific applied voltage. However, a small deviation from that bias leads to CT along with CAR contaminating that possibility.

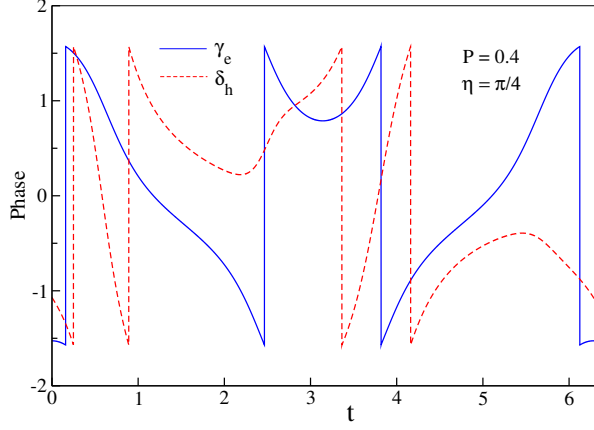


FIG. 3. (Color online) The plot shows the variation of the normal reflection phase γ_e and CAR phase δ_h with time t along a chosen pumping contour in the $\chi_1 - \chi_2$ plane.

The probability of non-local CAR process can be enhanced to unity (100%) by introducing two insulating barriers at each NS interfaces. We have considered $\mu_L = 5\Delta$, $\mu_R = -5\Delta$ and $\lambda_L = \lambda_R = 5\Delta$ which means that the Fermi level touches the bottom of the conduction band in the left normal silicene side while it touches the top of the valance band in right normal silicene side. The superconducting silicene side is doped with $\mu_S = 20\Delta$ to satisfy mean field condition for superconductivity $\mu_S \gg \Delta$ ²⁹. The band gaps λ_L and λ_R at the two normal sides can be adjusted by the external electric field E_z . The chosen value of the band gaps and doping levels permits one to neglect the contribution from the other valley (\mathbf{K}') which has much higher band gap compared to the other energy scales in the system. Under such circumstances, we obtain pure CAR in this setup with length of the superconducting side, $L = 2.1\xi$ (ξ is the phase coherence length of the superconductor) and incident electron energy, $E = 0.9\Delta$.

The reason behind obtaining pure CAR process in our NISIN set-up is as follows. As there is an band gap $2\lambda_L > \Delta$ in the left normal silicene side, probability for AR to take place is vanishingly small³¹. On the other hand, electron incident from the left side encounters a gap $2\lambda_R$ to tunnel through the other normal side prohibiting CT process to occur. The only possible scattering processes remain are normal reflection and CAR. Due

to the relativistic nature of Dirac fermions, both reflection and CAR probabilities are oscillatory as a function of the dimensionless insulating barrier strength. This allows our system to possess completely pure CAR process with probability one in $\chi_1 - \chi_2$ space. This resonant CAR peaks are $\pi/2$ periodic in nature. Such periodicity depends on the Fermi wave-length mismatch between the normal and superconducting region^{30,31}. Moreover, this periodicity is also clear from Fig. 4 where CAR probability is shown in the $\chi_1 - \chi_2$ plane. Note that the Fermi energy (chemical potential) need neither necessarily exactly touch valance band or conduction band nor they need to have same magnitude at the two normal regions to obtain pure CAR. We have chosen such parameter values only for simple visualization. A small deviation, from the numerical values that we have taken, leads to the 100% CAR probability to take place at other energy values.

As phases of the scattering amplitudes play a major role in the determination of the pumped charge, we show the behavior of phases of normal reflection and CAR amplitudes (γ_e and δ_h respectively) as a function of time for one full cycle in Fig. 3. We observe that both γ_e and δ_h exhibit four abrupt jumps for a full period of time (along a chosen contour). These jumps play a significant role in determining the pumped charge which we emphasis later. In addition, throughout our analysis, we have considered incident electrons to be normal to the interface *i.e.* $\alpha_{eL} = 0$ for simplicity. Later for completeness, we demonstrate angle dependance of the pumped charge.

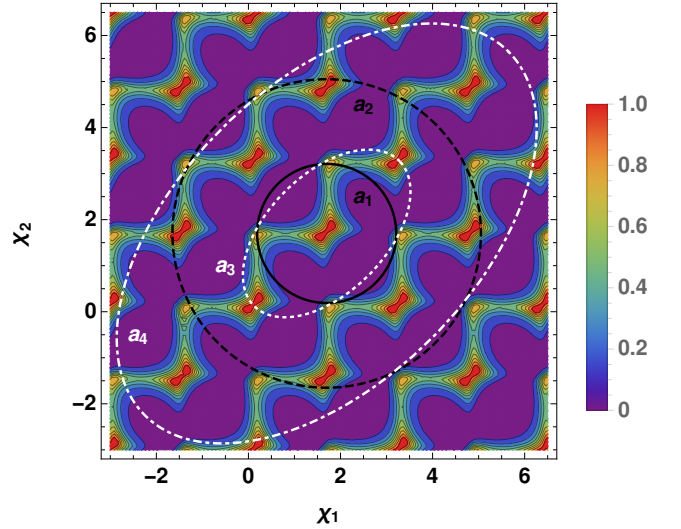


FIG. 4. (Color online) Plot of CAR probability $|t_A|^2$ in $\chi_1 - \chi_2$ plane. The contours a_1 , a_2 represents $\eta = \pi/4$ and $P = 1.51$, $P = 3.35$ respectively. On the other hand, the contours a_3 , a_4 are for $\eta = \pi/6$ and $P = 1.82$, $P = 4.56$ respectively. The value of the other parameters are chosen to be $L = 2.1\xi$, $E = 0.9\Delta$, $\omega = 1$, $\chi_0 = 1.7$, $\mu_L = 5\Delta$, $\mu_R = -5\Delta$, $\mu_S = 20\Delta$ and $\lambda_L = \lambda_R = 5\Delta$.

Under such scenario where the only possible scattering processes are normal reflection and CAR, Eq.(17) simpli-

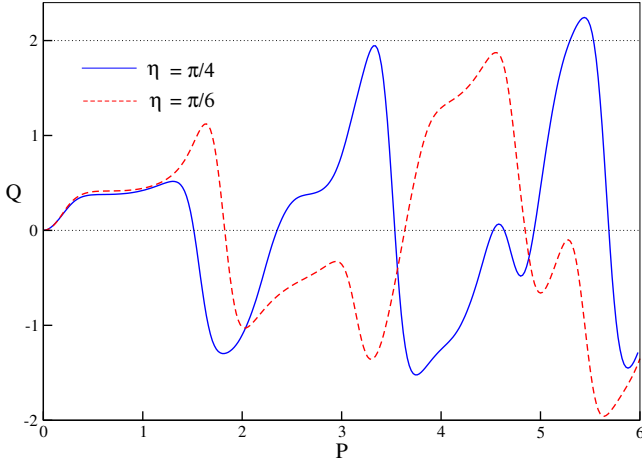


FIG. 5. (Color online) The pumped charge Q in units of the electron charge e , for pumping in the χ_1 - χ_2 plane, is shown as a function of the pumping strength P for circular and elliptic contours. The value of the other parameters are chosen to be the same as mentioned in Fig. 4.

fies to

$$Q = \frac{e}{2\pi} \int_0^T dt [-|t_A|^2 (\dot{\delta}_h \cos \alpha_{hR} + \dot{\gamma}_e \cos \alpha_{eL}) + \dot{\gamma}_e \cos \alpha_{eL}], \quad (18)$$

The behavior of pumped charge Q as a function of the pumping strength P is shown in Fig. 5 for $\eta = \pi/4, \pi/6$ which correspond to circular and elliptic contour respectively. The features of Q , depicted in Fig. 5, can be understood from the behavior of CAR probability $|t_A|^2$ in the χ_1 - χ_2 plane. For small values of P , pumped charge Q becomes vanishingly small in magnitude as the pumping contours do not enclose any $|t_A|^2 = 1$ point. When a pumping contour encloses one of the resonant peaks of $|t_A|^2$, topological part of the pumped charge gives rise to ne (n is the winding number) due to the integration around a singular point. At this point the reflection phase γ_e becomes ill-defined. However, the dissipative part nullifies the topological part resulting in small values of Q (see Eq.(17)) for both $\eta = \pi/4, \pi/6$. On the other hand, when a contour encloses both $|t_A|^2$ resonances, the relative integration direction around the two singular points plays an important role. Namely, when the two resonances are enclosed in a path with the same orientation, then the two contributions have opposite sign and tend to cancel each other. For *e.g.* when $\eta = \pi/4$ (black circular contours a_1 and a_2), the pumped charge is zero for $P = 1.51$ (see Fig. 5) as the contour a_1 encloses both the peaks resulting in zero pumped charge. Similar feature was found in case of resonant transmission in Ref. 37, 44, 48, and 66 where pumped charge was found to be zero when the pumping contour encloses both the resonances. Q approaches almost quantized value $2e$ for $P = 3.35$ and the corresponding contour a_2 encloses

even number of resonance peaks in the same orientation. Hence the topological part of pumped charge is almost zero and the contribution to Q arises from the dissipative part. The large contribution from the dissipative part arises due to the total drop of the CAR phase δ_h by a factor of 4π during its time evolution along the contour a_2 (see Fig. 3). Similarly, when $\eta = \pi/6$, Q is zero at $P = 1.82$ which corresponds to the a_3 contour which encloses four peaks in total, resulting in zero contribution from the topological part. On the other hand, pumped charge reaches its maximum when $P = 4.56$ (a_4 contour) where also the entire contribution originates from the dissipative part (see Fig. 5). Pumped charge changes sign depending on the sense of enclosing of the resonances *i.e.* whether it is clock-wise or anti-clockwise.

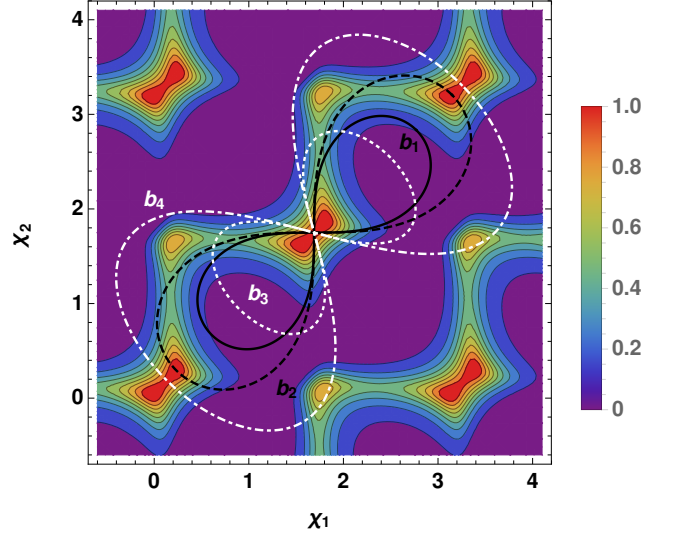


FIG. 6. (Color online) Plot of CAR probability $|t_A|^2$ along with lemniscate contours are shown in the χ_1 - χ_2 plane. The contours b_1, b_2 represents $\theta = \pi/4$ and the contours corresponding to $\theta = \pi/3$ are b_3, b_4 . We have chosen the mean values $\chi_{10} = 1.69$ and $\chi_{20} = 1.75$. The value of the other parameters are chosen to be the same as mentioned in Fig. 4.

The behavior of pumped charge Q with respect to the pumping strength P_L for lemniscate contours with $\theta = \pi/4$ and $\pi/3$ is presented in Fig. 7 and the corresponding contours are shown in Fig. 6. The pumped charge is small for small values of P_L where the contribution from topological part is cancelled by the dissipative part. As P_L increases, the corresponding pumping contour encloses both the $|t_A|^2$ peaks within opposite integration orientations and as a consequence, the two contributions for the pumped charge sum up. This is exactly the reason that motivates us to choose the lemniscate contours. However, the dissipative part effectively reduces the total pumped charge. Such feature arises for lemniscate contours of the type b_1 and b_3 . Moreover, we observe that the pumped charge becomes zero for $P_L = 2.06$ at $\theta = \pi/4$, where both the bubbles of the b_2 contour enclose two $|t_A|^2$ peaks from the two adjacent resonances in the χ_1 - χ_2 plane and hence their com-

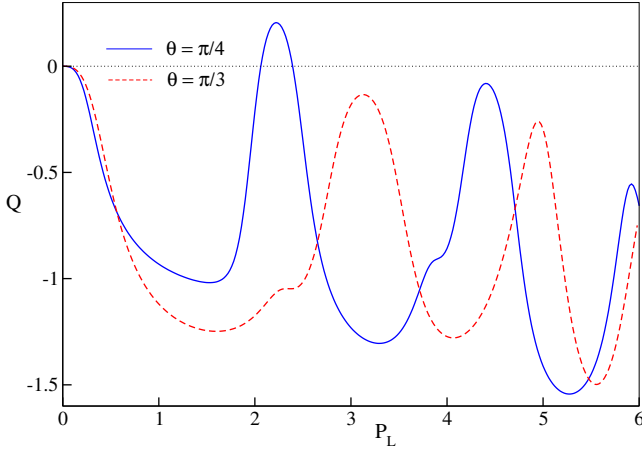


FIG. 7. (Color online) Pumped charge Q in unit of electron charge e , for pumping in the χ_1 - χ_2 plane, is shown as a function of the pumping strength P_L for the lemniscate contours. All other parameters are identical to those used in Fig. 4.

bined contribution to pumped charge get cancelled for each bubble separately. The qualitative behavior of Q remains similar for $\theta = \pi/3$ where maximum value of Q is achieved when each bubble of the lemniscate contour of type b_4 encloses odd number of resonances while Q tends to zero as even number of peaks are enclosed by each bubble of the contour.

B. Pumping via transmission/CT in the χ_1 - χ_2 plane

In this subsection we present our numerical results of adiabatic quantum pumping through pure CT *i.e.* resonant transmission process. The latter can be achieved by tuning the Fermi level (chemical potential) at the bottom of the conduction band in both the normal silicene regions. The numerical values of all the parameters are identical to those used before except now $\mu_R = 5\Delta$. To obtain perfect transmission in this regime, length of the superconducting region and incident electron energies are chosen to be $L = 2.2\xi$ and $E = 0.93\Delta$.

As before, due to the presence of a gap ($\lambda_L > \Delta$) in the left normal side, AR is forbidden while CAR cannot take place because of the unavailability of the hole states in the right normal region in the low energy limit. An incident electron thus only encounters two scattering processes which are normal reflection and transmission. The presence of insulating barriers between the NS interfaces allows both these scattering probabilities to be oscillatory as a function of the dimensionless barrier strengths χ_1 and χ_2 which is depicted in Fig. 9.

In this regime, as AR and CAR probabilities are always zero, hence Eq.(17) reduces to

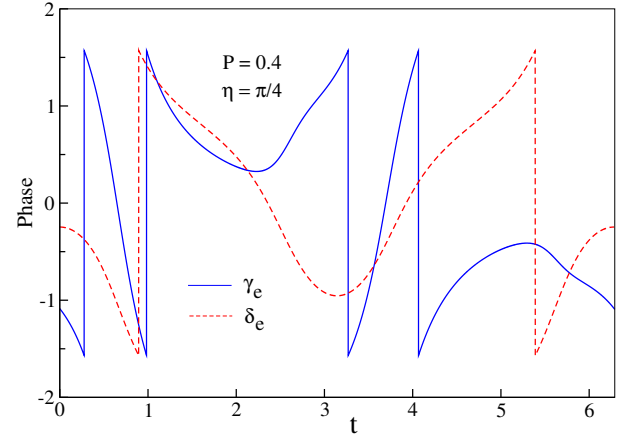


FIG. 8. (Color online) The variation of the normal reflection phase γ_e and transmission phase δ_e with time t is shown along a chosen pumping contour in the χ_1 - χ_2 plane.

$$Q = \frac{e}{2\pi} \int_0^T dt [|t_e|^2 (\dot{\delta}_e \cos \alpha_{eR} - \dot{\gamma}_e \cos \alpha_{eL}) + \dot{\gamma}_e \cos \alpha_{eL}] , \quad (19)$$

In Fig. 8, we show the behavior of reflection phase γ_e and transmission phase δ_e as a function of time for one full period. Note that, γ_e and δ_e come across four and two abrupt jumps respectively over the full cycle. The consequences of these jumps in determining the pumped charge will be discussed later.

In Fig. 10, pumped charge Q is presented as a function of pumping strength P for $\eta = \pi/4$ and $\pi/6$. The latter represents circular and elliptic contours respectively. To understand the behavior of the pumped charge, we also investigate the transmission probability $|t_e|^2$ in χ_1 - χ_2 plane. In Fig. 9, we plot $|t_e|^2$ together with different possible circular and elliptic pumping contours. We observe, as before, pumped charge is very tiny when P is small. As the pumping contour encloses only one resonant transmission peak at which the reflection phase γ_e becomes singular, topological part of the pumped charge gives rise to the quantized value e . However, the dissipative part reduces the pumped charge from its quantized value. With the enhancement of P , pumping contour starts enclosing both the transmission peaks leading to zero contribution to the pumped charge. This feature can be seen to occur at $P = 1.5$ for $\eta = \pi/4$ (c_1 contour) where total pumped charge is zero (see Fig. 10). At this P value, over a full period of time, reflection and transmission phases γ_e and δ_e respectively cancel each other and thus the dissipative part also vanishes (see Eq.(19)). Q approaches to $-e$ at $P = 3.34$ where the topological part of the pumped charge is zero and the total contribution comes from the dissipative part. The reason behind null contribution from topological part is that the contour c_2 encloses even number of peaks, all in a path with the same orientation. However, the finite contribution from

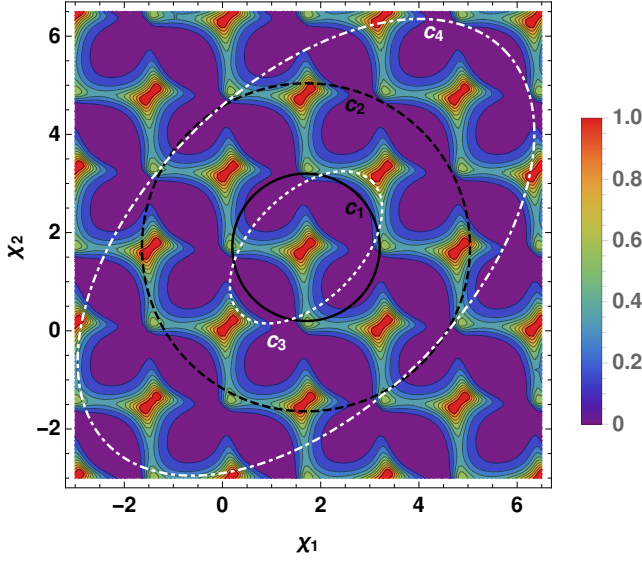


FIG. 9. (Color online) Transmission probability $|t_e|^2$ along with circular and elliptic contours are shown in χ_1 - χ_2 plane. The contours c_1 , c_2 represent $\eta = \pi/4$ and $P = 1.5$, $P = 3.34$ respectively. On the other hand, the contours c_3 , c_4 correspond to $\eta = \pi/6$ and $P = 1.55$, $P = 4.65$ respectively. The value of the other parameters are chosen to be $L = 2.2\xi$, $E = 0.93\Delta$, $\omega = 1$, $\chi_0 = 1.7$, $\mu_L = 5\Delta$, $\mu_R = 5\Delta$, $\mu_S = 20\Delta$ and $\lambda_L = \lambda_R = 5\Delta$.

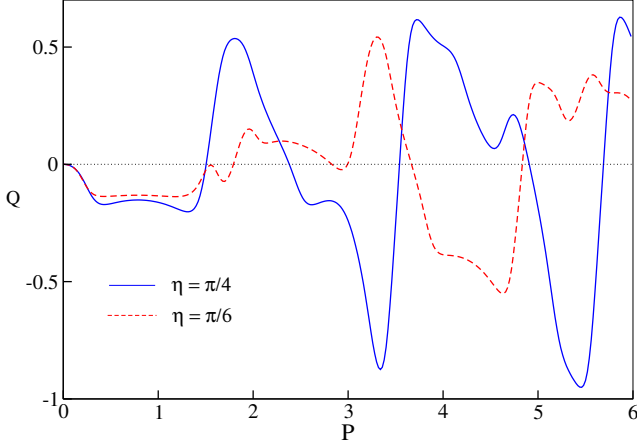


FIG. 10. (Color online) Pumped charge Q in unit of electron charge e , for pumping in the χ_1 - χ_2 plane, is shown as a function of the pumping strength P for the circular and elliptic contours. We choose the same values of the other parameters as mentioned in Fig. 9.

the dissipative part emerges due to the total jump of the transmission phase δ_e by a factor of 2π during its time evolution along the contour c_2 (see Fig 8). The behavior is analogous in case of elliptic contour *i.e.* $\eta = \pi/6$ where we see from Fig. 10 that the pumped charge is zero for $P = 1.55$ as the corresponding contour c_3 in Fig. 9 encloses two resonances with the same orientation. However, the maximum value of pumped charge for $\eta = \pi/6$ reaches about $Q \simeq 0.6e$ at $P = 4.65$ for which the corre-

sponding contour c_4 encloses even number of peaks in the same sense leading to zero contribution from topological part (see Fig. 10). In this case also the finite value of pumped charge arises from the dissipative part.

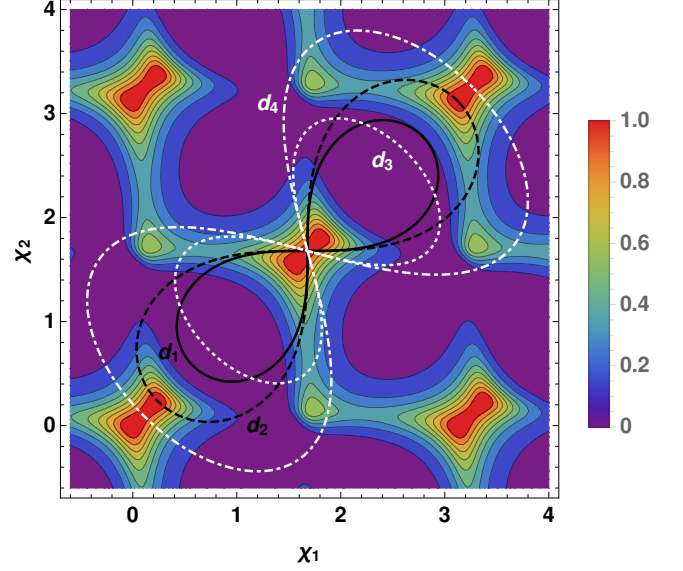


FIG. 11. (Color online) Transmission probability $|t_e|^2$ together with different lemniscate contours are shown in the χ_1 - χ_2 plane. The contours d_1 , d_2 represents $\theta = \pi/4$ and the contours d_3 , d_4 corresponds to $\theta = \pi/3$. We choose the values of χ_{10} and χ_{20} as $\chi_{10} = \chi_{20} = 1.68$. All other parameters are identical to those used in Fig. 9.

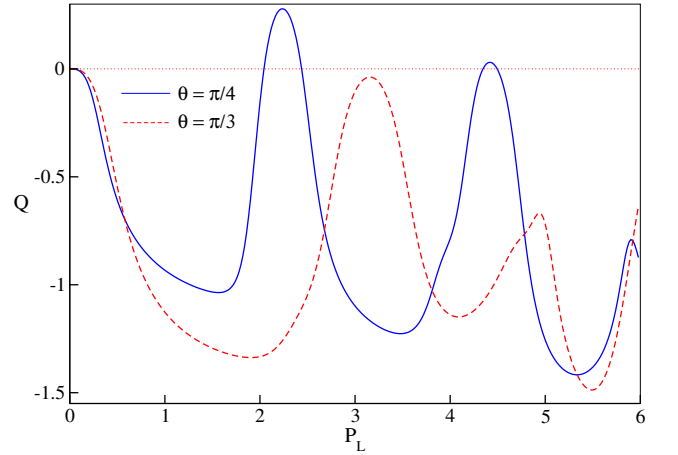


FIG. 12. (Color online) Pumped charge Q in unit of electron charge e is depicted as a function of the pumping strength P_L for the lemniscate contours. All other parameters are identical to those used in Fig. 9.

In Fig. 11, we show the behavior of pumped charge Q as a function of pumping strength P_L with lemniscate contours. To understand the corresponding behavior of Q , we also show $|t_e|^2$ in the χ_1 - χ_2 plane along with different lemniscate contours. As the two resonances are enclosed in opposite orientations, the topological part gives

rise to $2e$ due to the addition of the integration around two singular points in opposite paths. This is achieved by the d_1 contour ($P_L = 1.56$, $\theta = \pi/4$) as shown in Fig. 11. However the maximum value of Q approaches $-e$ due to the finite contribution coming from the dissipative part which effectively reduces the total pumped charge. On the other hand, pumped charge becomes vanishingly small when each bubble of the lemniscate contour encloses even number of transmission resonances with the same orientation. Due to this reason, we obtain $Q = 0$ for $P_L = 2.04$ as shown in Fig. 12 and the corresponding contour d_2 encloses four $|t_e|^2$ peaks in total, two by each bubble of the contour, leading to zero pumped charge. We observe similar features in Q by considering different value of θ , *i.e.* $\theta = \pi/3$ corresponding to the contours d_3 and d_4 in Fig. 11.

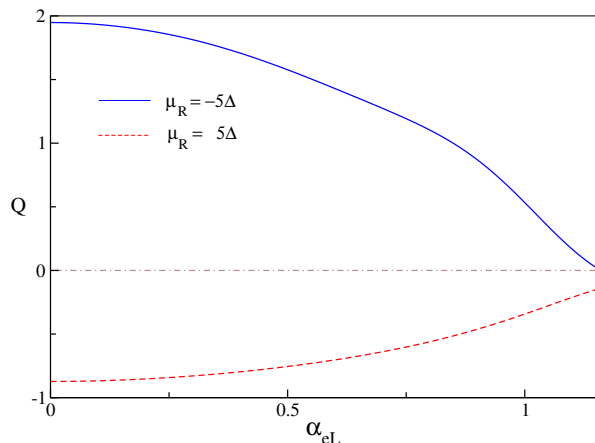


FIG. 13. (Color online) Pumped charge Q in unit of electron charge e is shown as a function of the incident angle α_{eL} for both $\mu_R = -5\Delta$ and $\mu_R = 5\Delta$. Here we choose $\eta = \pi/4$, $P = 3.35$ for $\mu_R = -5\Delta$ and $P = 3.34$ for $\mu_R = 5\Delta$ respectively.

As we mention earlier, the above mentioned results are valid for normal incidence of the incoming electron *i.e.* $\alpha_{eL} = 0$. Here, we explore the dependence of the pumped charge on the angle of incident electrons. In Fig. 13, pumped charge Q as a function of incident angle α_{eL} is presented when either CAR probability $|t_A|^2$ or transmission probability $|t_e|^2$ is enclosed by the circular pumping contour. The α_{eL} dependence is shown upto the critical angle α_c . Above α_c , AR and CAR processes cannot take place⁶⁹. Rather, normal reflection is the dominating scattering mechanism above α_c . It is evident from Fig. 13 that as the angle of incidence α_{eL} increases, Q decreases monotonically for enclosing $|t_A|^2$ or $|t_e|^2$ in either cases. The reason can be attributed to the fact that both $|t_A|^2$ and $|t_e|^2$ in the two different scenarios, acquire the maximum value at normal incidence *i.e.* $\alpha_{eL} = 0$ and decreases slowly with the increase of α_{eL} . Also, for $0 < \alpha_{eL} < \alpha_c$, normal reflection probability $|r_e|^2$ also contributes to Eq.(17) and the interplay between all the quantum mechanical amplitudes and their phases results in smaller value of pumped charge. Note that, in case of pumping via CAR resonance process in $\chi_1 - \chi_2$ plane, Q

approaches zero as α_{eL} proceeds towards α_c . However, Q is finite even at α_c in case of pumping via resonant transmission in the same parameter space, This is because at α_c , $|t_A|^2$ vanishes while $|t_e|^2$ still has small probability which gives rise to small but finite pumped charge from the dissipative part (see Eq.(19)).

IV. SUMMARY AND CONCLUSIONS

To summarize, in this article, we have investigated the possibility of enhancing the CAR probability $|t_A|^2$ in silicene NSN set up by introducing thin insulating barrier^{30,31} I at each NS interface. We show that, for electrons with normal incidence, 100% CAR probability can be obtained in our setup by tuning the band gap in both the normal silicene regions by applying an external electric field as well as adjusting the chemical potential by additional gate voltages in both the normal sides. We also show that $|t_A|^2$ is periodic in $\chi_1 - \chi_2$ plane due to relativistic nature of Dirac fermions. On the other hand, it is also possible to attain transmission probability $|t_e|^2$ of magnitude unity in silicene NISIN junction under suitable circumstances. Owing to Dirac nature of particles, $|t_e|^2$ also exhibits periodic behavior in the space of barrier strengths χ_1 and χ_2 .

We then explore adiabatic quantum charge pumping through our NISIN setup and show that the behavior of pumped charge as a function of the pumping strength P is closely related to the features of CAR probability $|t_A|^2$ or transmission probability $|t_e|^2$ in the pumping parameter space. For electrons with normal incidence, quantized pumped charge with maximum value close to $Q \simeq 2e$ can be obtained when particular circular or elliptic pumping contour encloses the resonant CAR in $\chi_1 - \chi_2$ plane. Although the major contribution to Q , in this case, arises from the dissipative part. On the other hand, integer pumped charge can also be obtained with lemniscate contour when odd number of $|t_A|^2$ peaks are enclosed by each of its bubble. The maximum value of pumped charge approaches $Q \simeq -e$ when various pumping contours enclose $|t_e|^2$ resonance in the same parameter space. However, pumped charge decreases monotonically as we increase the angle of incidence of the incoming electron.

As far as practical realization of our silicene NISIN quantum pumping set up is concerned, superconductivity in silicene may be possible to induce by proximity coupled to a *s*-wave superconductor for *e.g.* Al analogous to graphene^{73,74}. Once such proximity induced superconductivity in silicene is realized, fabrication of silicene NISIN junction can be feasible. The strength of the two oscillating barriers can be possible to tune by applying a.c gate voltages. Typical spin-orbit energy in silicene is $\lambda_{SO} \sim 4$ meV and the buckling parameter is $l \approx 0.23$ Å^{3,5}. Considering Ref. 73 and 75, typical proximity induced superconducting gap in silicene would be $\Delta \sim 0.2$ meV. For such induced superconducting gap, chemical potential is $\mu_S \sim 20\Delta \sim 4$ meV and we obtain

$\xi \sim 580$ nm and length of the superconducting region $L \sim 1.2$ μm . Hence, an insulating barrier of thickness $d \sim 10 - 20$ nm may be considered as thin barrier and the gate voltage $V_0 \sim 500$ meV can therefore justify the needs of our model³⁰. To achieve both the resonances, $\lambda_L = \lambda_R = 5\Delta \sim 1$ meV which can be tuned by an external electric field $E_z \sim 200$ V/ μm . For both resonant processes, typical dwell time of the electrons inside the superconducting region is ~ 2.2 fs while the time period

of the oscillating barriers is $T \sim 30$ ps and the corresponding frequency of modulation parameters turns out to be ~ 230 GHz. Thus the dwell time τ_{dwell} is much smaller than the time period T of the modulation parameters, hence satisfying the adiabatic condition of quantum pump. Pumped current through our setup should be in the range of $\sim 10 - 15$ nA which can be measurable in modern day experiment.

-
- ¹ A. K. Geim and K. S. Novoselov, Nat. Materials **6**, 183 (2007).
 - ² A. H. Castro Neto, F. Guinea, N. M. R. Peres, K. S. Novoselov, and A. K. Geim, Rev. Mod. Phys. **81**, 109 (2009).
 - ³ C.-C. Liu, H. Jiang, and Y. Yao, Phys. Rev. B **84**, 195430 (2011).
 - ⁴ M. Houssa, A. Dimoulas, and A. Molle, J. Phys. Cond. Matt. **27**, 253002 (2015).
 - ⁵ M. Ezawa, J. Phys. Soc. Jpn. **84**, 121003 (2015).
 - ⁶ A. Hattori, S. Tanaya, K. Yada, M. Araidai, M. Sato, Y. Hatsugai, K. Shiraishi, and Y. Tanaka, arXiv:1604.04717 [cond-mat.mes-hall].
 - ⁷ T. P. Kaloni, G. Schreckenbach, M. S. Freund, and U. Schwingenschlöggl, Phys. Status Solidi RRL **10**, 133 (2016).
 - ⁸ B. Lalmi, H. Oughaddou, H. Enriquez, A. Kara, S. Vizzini, B. Ealet, and B. Aufray, Appl. Phys. Lett. **97**, 223109 (2010).
 - ⁹ P. D. Padova *et al*, Appl. Phys. Lett. **96**, 261905 (2010).
 - ¹⁰ P. Vogt, P. D. Padova, C. Quaresima, J. Avila, E. Frantzeskakis, M. C. Asensio, A. Resta, B. Ealet, and G. L. Lay, Phys. Rev. Lett. **108**, 155501 (2012).
 - ¹¹ C.-L. Lin, R. Arafune, K. Kawahara, N. Tsukahara, E. Minamitani, Y. Kim, N. Takagi, and M. Kawai, Appl. Phys. Exp. **5**, 045802 (2012).
 - ¹² C. C. Liu, W. Feng, and Y. Yao, Phys. Rev. Lett. **107**, 076802 (2011).
 - ¹³ M. Ezawa and N. Nagaosa, Phys. Rev. B **88**, 121401(R) (2013).
 - ¹⁴ M. Ezawa, Phys. Rev. B **87**, 155415 (2013).
 - ¹⁵ M. Ezawa, Eur. Phys. J. B **85**, 363 (2012).
 - ¹⁶ M. Ezawa, Phys. Rev. Lett. **114**, 056403 (2015).
 - ¹⁷ T. P. Kaloni, N. Singh, and U. Schwingenschlöggl, Phys. Rev. B **89**, 035409 (2014).
 - ¹⁸ N. Drummond, V. Zolyomi, and V. Fal'Ko, Phys. Rev. B **85**, 075423 (2012).
 - ¹⁹ M. Ezawa, New J. Phys. **14**, 033003 (2012).
 - ²⁰ I. Zutić, J. Fabian, and S. Das Sarma, Rev. Mod. Phys. **76**, 323 (2004).
 - ²¹ Y. Wang, J. Zheng, Z. Ni, R. Fei, Q. Liu, R. Quhe, C. Xu, J. Zhou, Z. Gao, and J. Lu, Nano **7**, 1250037 (2012).
 - ²² Y. Wang, R. Quhe, D. Yu, J. Li, and J. Lu, Chin. Phys. B **24**, 087201 (2015).
 - ²³ W.-F. Tsai, C.-Y. Huang, T.-R. Chang, H. Lin, H.-T. Jeng, and A. Bansil, Nat. Commn. **4**, 1500 (2013).
 - ²⁴ S. Rachel and M. Ezawa, Phys. Rev. B **89**, 195303 (2014).
 - ²⁵ H. Pan, Z. Li, C.-C. Liu, G. Zhu, Z. Qiao, and Y. Yao, Phys. Rev. Lett. **112**, 106802 (2014).
 - ²⁶ T. Yokoyama, Phys. Rev. B **87**, 241409(R) (2013).
 - ²⁷ R. Saxena, A. Saha, and S. Rao, Phys. Rev. B **92**, 245412 (2015).
 - ²⁸ L. Tao, E. Cinquanta, D. Chiappe, C. Grazianetti, M. Fanciulli, M. Dubey, A. Molle, and D. Akinwande, Nat. Nanotechnol. **10**, 227 (2015).
 - ²⁹ J. Linder and T. Yokoyama, Phys. Rev. B **89**, 020504(R) (2014).
 - ³⁰ G. C. Paul, S. Sarkar, and A. Saha, arXiv:1608.03483 [cond-mat.mes-hall].
 - ³¹ S. Sarkar, A. Saha, and S. Gangadharaiyah, arXiv:1609.00693 [cond-mat.mes-hall].
 - ³² D. Thouless, Phys. Rev. B **27**, 6083 (1983).
 - ³³ M. Büttiker, H. Thomas, and A. Prêtre, Z. Phys. B **94**, 133 (1994).
 - ³⁴ P. Brouwer, Phys. Rev. B **58**, R10135 (1998).
 - ³⁵ P. Brouwer, Phys. Rev. B **63**, 121303 (2001).
 - ³⁶ A. Kundu, S. Rao, and A. Saha, Phys. Rev. B **83**, 165451 (2011).
 - ³⁷ A. Saha, D. Rainis, R. P. Tiwari, and D. Loss, Phys. Rev. B **90**, 035422 (2014).
 - ³⁸ Q. Niu, Phys. Rev. Lett. **64**, 1812 (1990).
 - ³⁹ I. Aleiner and A. Andreev, Phys. Rev. Lett. **81**, 1286 (1998).
 - ⁴⁰ T. Shutenko, I. Aleiner, and B. Altshuler, Phys. Rev. B **61**, 10366 (2000).
 - ⁴¹ M. Moskalets and M. Büttiker, Phys. Rev. B **66**, 205320 (2002).
 - ⁴² M. Moskalets and M. Büttiker, Phys. Rev. B **69**, 205316 (2004).
 - ⁴³ O. Entin-Wohlman, A. Aharony, and Y. Levinson, Phys. Rev. B **65**, 195411 (2002).
 - ⁴⁴ O. Entin-Wohlman and A. Aharony, Phys. Rev. B **66**, 035329 (2002).
 - ⁴⁵ R. Benjamin and C. Benjamin, Phys. Rev. B **69**, 085318 (2004).
 - ⁴⁶ C. Benjamin and R. Citro, Phys. Rev. B **72**, 085340 (2005).
 - ⁴⁷ S. Das and S. Rao, Phys. Rev. B **71**, 165333 (2005).
 - ⁴⁸ S. Banerjee, A. Mukherjee, S. Rao, and A. Saha, Phys. Rev. B **75**, 153407 (2007).
 - ⁴⁹ A. Agarwal and D. Sen, J. Phys. Cond. Matt. **19**, 046205 (2007).
 - ⁵⁰ A. Agarwal and D. Sen, Phys. Rev. B **76**, 235316 (2007).
 - ⁵¹ R. P. Tiwari and M. Blaauboer, Appl. Phys. Lett. **97**, 243112 (2010).
 - ⁵² R. Zhu and H. Chen, Appl. Phys. Lett. **95**, 122111 (2009).
 - ⁵³ J. Splettstoesser, M. Governale, and J. König, Phys. Rev. B **77**, 195320 (2008).
 - ⁵⁴ S. Rojek, M. Governale, and J. König, Phys. Status Solidi B **251**, 1912 (2014).
 - ⁵⁵ M. Switkes, C. Marcus, K. Campman, and A. Gossard,

- Science **283**, 1905 (1999).
- ⁵⁶ P. Leek, M. Buitelaar, V. Talyanskii, C. Smith, D. Anderson, G. Jones, J. Wei, and D. Cobden, Phys. Rev. Lett. **95**, 256802 (2005).
 - ⁵⁷ S. K. Watson, R. Potok, C. Marcus, and V. Umansky, Phys. Rev. Lett. **91**, 258301 (2003).
 - ⁵⁸ M. Buitelaar, V. Kashcheyevs, P. Leek, V. Talyanskii, C. Smith, D. Anderson, G. Jones, J. Wei, and D. Cobden, Phys. Rev. Lett. **101**, 126803 (2008).
 - ⁵⁹ F. Giazotto, P. Spathis, S. Roddaro, S. Biswas, F. Taddei, M. Governale, and L. Sorba, Nat. Phys. **7**, 857 (2011).
 - ⁶⁰ M. Blumenthal, B. Kaestner, L. Li, S. Giblin, T. Janssen, M. Pepper, D. Anderson, G. Jones, and D. Ritchie, Nat. Phys. **3**, 343 (2007).
 - ⁶¹ E. Prada, P. San-Jose, and H. Schomerus, Phys. Rev. B **80**, 245414 (2009).
 - ⁶² M. Alos-Palop and M. Blaauboer, Phys. Rev. B **84**, 073402 (2011).
 - ⁶³ R. Citro, F. Romeo, and N. Andrei, Phys. Rev. B **84**, 161301 (2011).
 - ⁶⁴ M. Alos-Palop, R. P. Tiwari, and M. Blaauboer, New. J. Phys. **14**, 113003 (2012).
 - ⁶⁵ J. E. Avron, A. Elgart, G. M. Graf, and L. Sadun, Phys. Rev. Lett. **87**, 236601 (2001).
 - ⁶⁶ Y. Levinson, O. Entin-Wohlman, and P. Wölfle, Physica A **302**, 335 (2001).
 - ⁶⁷ M. Gibertini, R. Fazio, M. Polini, and F. Taddei, Phys. Rev. B **88**, 140508(R) (2013).
 - ⁶⁸ P. L. S. Lopes, P. Ghaemi, S. Ryu, and T. L. Hughes, arXiv:1609.02565 [cond-mat.mes-hall].
 - ⁶⁹ C. W. J. Beenakker, Phys. Rev. Lett. **97**, 067007 (2006).
 - ⁷⁰ C. W. J. Beenakker, Rev. Mod. Phys. **80**, 1337 (2008).
 - ⁷¹ A. Kundu, S. Rao, and A. Saha, Phys. Rev. B **82**, 155441 (2010).
 - ⁷² J. Cayssol, Phys. Rev. Lett. **100**, 147001 (2008).
 - ⁷³ H. B. Heersche, P. Jarillo-Herrero, J. B. Oostinga, L. M. K. Vandersypen, and A. F. Morpurgo, Nature **446**, 56 (2007).
 - ⁷⁴ J.-H. Choi, G.-H. Lee, S. Park, D. Jeong, J.-O. Lee, H.-S. Sim, Y.-J. Doh, and H.-J. Lee, Nat. Commun. **4**, 2525 (2013).
 - ⁷⁵ V. E. Calado, S. Goswami, G. Nanda, M. Diez, A. R. Akhmerov, K. Watanabe, T. Taniguchi, T. M. Klapwijk, and L. M. K. Vandersypen, Nat. Nanotechnol. **10**, 761 (2015).